Analog study of bifurcation structures in a Van der Pol oscillator with a nonlinear restoring force

Yao-Huang Kao*
Department of Communication Engineering, National Chiao-Tung University, Hsinchu, Taiwan 30050, Republic of China

Ching-Sheu Wang
Institute of Electro-Optical Engineering, National Chiao-Tung University, Hsinchu, Taiwan 30050, Republic of China and Telecommunication Laboratories, Ministry of Transportation and Communication, Yang-Mei, Taoyuan, Taiwan, Republic of China

(Received 20 January 1993)

The injection locking and chaotic transitions in a Van der Pol oscillator with a nonlinear-restoring-force term were investigated in this article via an electronic circuit. Three types of locking processes were differentiated from each other in light of local and global bifurcations. The influences of the nonlinear restoring force on the bifurcation structure were also discussed.

PACS number(s): 02.50.−r, 42.50.Lc, 42.55.Px, 42.60.Fc

I. INTRODUCTION

The nonlinear dynamics in forced systems have received a substantial amount of attention since the prediction of the scaling constants of routes of chaos. Two of the fundamental forced oscillators, Duffing and Van der Pol oscillators (VDP), have been extensively examined because a number of dynamic features embedded in the physical systems can be realized from these two systems [1–13]. The equations of motion in Duffing and VDP oscillators are

$$\ddot{x}+\mu\dot{x}+(\alpha-\gamma x^2)x=F\sin(\Omega t) \tag{1}$$

and

$$\ddot{x}+\mu(x^2+g)\dot{x}+\alpha x=F\sin(\Omega t)\ , \tag{2}$$

respectively. The former has the nonlinear-restoring-force $(\alpha-\gamma x^2)x$ and linear damping terms. The latter has the nonlinear damping term $\mu(x^2+g)\dot{x}$ and linear restoring force and can also contain a free-running solution or relaxation oscillation, depending on the sign of the g factor in the damping term. The chaotic dynamics in Duffing oscillator involves the period-doubling route to chaos, intermittency, and crisis event [3,4]. Its bifurcation structure reveals as swallow-tailed shapes among the resonant regions [4,5]. The dynamical behaviors in VDP oscillator have also been studied by several authors. The regular case with small coefficient μ has been studied analytically with the averaging and topological methods [6–9]. The chaotic phenomena have been indicated to not occur for damping coefficient $\mu<1$ and can occur with the linear restoring force replaced by a cubic or quantic nonlinear-restoring-force term [10,11]. The chaos, devil's staircase, Fractal dimension, Farey tree, period-doubling route and equal-period bifurcation have also been indicated with $\mu\gg1$ [12,13]. In physical systems containing the limit cycles, they may actually have rather complicated nonlinear-restoring-force terms in their equations of motion [14–21]. In this paper we examine the dynamical transitions in periodically forced self-oscillating systems containing a cubic term in the restoring force as follows:

$$\ddot{x}+\mu(x^2+g)\dot{x}+\alpha x-\gamma x^3=F\sin(\Omega t)\ . \tag{3}$$

This equation is a mixed type of Duffing and VDP oscillators. Regarding the nonlinear optics, Eq. (3) is often used to model the optical bistability in a dispersive medium, in which the refractive index is dependent of the optical intensity, or the bistability in the gain-suppression–saturable-absorber medium, in which the gain or loss is saturated as intensity is increased. An interesting case is the dynamics of optical bistability in laser diode irradiated by external light [14,15]. The laser diode functions as an injection-locked oscillator or just only a passive Fabry-Pérot cavity with the nonlinear medium, depending on the dc bias current above or below the threshold, respectively. Besides that, the system described by Eq. (3) is denoted as a Bonhoeffer oscillator in the field of biology, where the propagation of an electronic pulse along the membranes of a nerve cell is discussed [18]. Thus, the study of the dynamics in Eq. (3) is not only of theoretical but also of practical interest.

Basically, Eq. (3) contains a free-running solution with a certain amplitude for $g<0$. The injection locking occurs as the driving frequency is near or in synchronization with the natural frequency or its integral multiple or submultiple. The studies of the nonlinear behaviors, according to the authors' knowledge, can be classified into two categories. One category investigates the features of steady states and the other finds the transient processes under the variation of controlling parameters [1,2]. For the steady states the winding number λ, which is the ratio of the free-running frequency to the excitation frequency, is conveniently adopted for describing the locking behaviors. The number $\lambda=p/q$ is rational as the system becomes locked to an external signal, and is irrational for the unlocked case. This number reveals the feature of the Farey tree with a new frequency locked at $\lambda=(p+r)/(q+s)$ between two adjacent locked states at $\lambda=p/q$ and r/s. The two numbers $\lambda=p/q$ and r/s must

satisfy the relation of $|ps-rq|=1$. Furthermore, the winding number forms a devil's staircase at a specific parameter region. The dimension of the related attractor is expected to be a noninteger. The universal features have actually been predicted from studying a simple map of the circle onto itself [22]. The Poincaré section, which is developed by stroboscopically sampling the solution one point per cycle, is often adopted in continuous systems in order to test the universal features. The reduced dimension-one attractor exhibits a fixed point for the limiting cycle, an invariant circle for the quasiperiodic solution, and broken and folded sets for the chaotic solution. The occurrence of chaos is linked to the destruction of invariant circles.

Two types of local and global bifurcations are involved in the transition process, which can be classified according to the topological change of the attractors [2]. In the local bifurcation of codimension-one with only one control parameter variation, there are saddle-node, pitchfork, flip, and Hopf bifurcations and have the Floquet multiplier passing the unit circle from $+1$, $+1$, -1, and a complex number, respectively. The global bifurcations are associated with a topological change of the invariant manifolds of a saddle point. Two types of blue-sky catastrophe and intermittent catastrophe are often encountered. The former is the global bifurcation proper, which is the qualitative change of invariant manifold topology. The latter is a hybrid type, in which the bifurcation is a local bifurcation of the catastrophic variety, whose full repercussions are determined by global structure of invariant manifolds, and this is referred as local and global bifurcations. The local and global bifurcations in Eq. (3) are extensively examined here. Although the complicated behaviors are expected at a high μ value and high excitation similar to the VDP system, the lightly damped case with $\mu<1$ is focused to signify the role of the nonlinear restoring force on the chaotic dynamics.

So as to prevent the waiting for the long transient periods in computations, an analog circuit using the operational amplifiers and multipliers is constructed in searching for the various transitions. The principle advantage of the electronic analog lies in its fast response as the controlled parameters are changed. An auxiliary circuit is also constructed for performing the Poincaré section and return maps, from which the types of bifurcations can be directly differentiated on the scope. The distinction of intermittent catastrophe and blue-sky catastrophe, which are cumbersome in numerical computations, can thus be instantly found with this tool.

This paper is organized as follows. The electronic circuit of analog simulator is briefly described in Sec. II. Those experimental results are presented in Sec. III, which involve different transitions of bifurcation which have been extensively searched in the parameter space. Not only the steady-state attractors but also the transitions of the attractors are presented. The concluding remarks are finally made in Sec. IV.

II. ELECTRONIC ANALOG CIRCUIT

The electronic simulator for Eq. (3) can be easily constructed by the conventional operational amplifiers (LM741) and four-quadrant multipliers (AD534). The dc offset voltages are controlled to within mV order to minimize the effects of dc offset. The schematic diagram is shown in Fig. 1 with output voltage V satisfying the differential equation as

$$\ddot{V}=\frac{0.1}{RC}\dot{V}-\frac{0.1V^2}{(RC)^5}\dot{V}+\frac{0.1}{(RC)^6}V^3-\frac{1}{(RC)^2}V+F\sin(2\pi ft)\ , \tag{4}$$

where RC is the time constant of the integrators, f is the driving frequency, and dot is the derivative with respect to time t. By setting $X=V/(RC)^2$ and $\tau=t/RC$, Eq. (4) becomes

$$\frac{dX^2}{d\tau^2}+0.1(X^2-1)\frac{dX}{d\tau}+X-0.1X^3=F\sin(\Omega\tau)\ , \tag{5}$$

where the frequency $\Omega=f/f_0$ is normalized by the characteristic frequency $f_0=1/2\pi RC$ ($=162.2$ Hz) of the circuit. The coefficients are intentionally chosen to match the coefficients of Eq. (3) with $\mu=0.1$, $g=-1$, $\alpha=1$, and $\gamma=0.1$. The output voltage is sampled stroboscopically to form a Poincaré section $(x(n),\dot{x}(n))=(x(\tau),\dot{x}(\tau))$ at $\tau=2n\pi$, n is an integer, and the return maps defined as $P:(x(n))\rightarrow(x(n+1))$ with the auxiliary circuit containing two samples and holders. The Poincaré section reveals q dots for every p cycles for the locked states with $\lambda=p/q$ and an invariant circle for the quasiperiodic state. The instability, especially for the quasiperiodic and chaotic attractors, can be directly distinguished from the slope at the intersection point with the diagonal. The results are presented in the subsequent sections.

III. EXPERIMENTAL RESULTS

The dynamic phenomena in Eq. (3) include the injection locking, multiple hysteresis, period-doubling route,

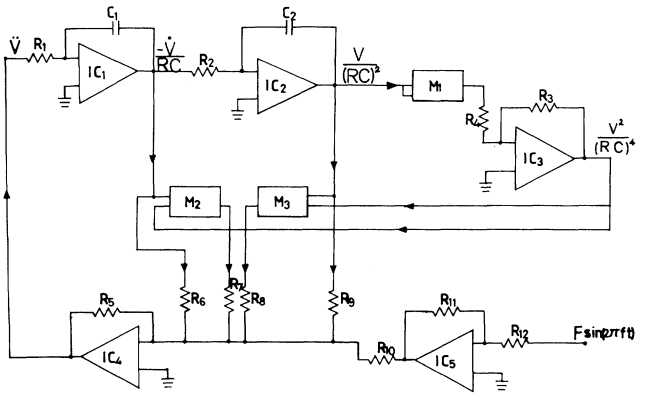

FIG. 1. The schematic diagram for Eq. (3). IC_1 and IC_2 (LM741) are operational integrators with $V_0=(-1/RC)\int\dot{V}\,dt$. The resistances and capacitances are set as $R=R_1=R_2=10$ kΩ and $C=C_1=C_2=0.0982$ μF. The resistors $R_3=R_6=100$ kΩ and the others are equal to 10 kΩ. M_1, M_2, and M_3 are multipliers (AD534) with output $-XY/10$ for input X and Y. The free-running frequency f_0 is 135.525 Hz.

intermittent hopping, and crisis [23]. Because of the coexisting multiattractors, the dynamical transitions are traced out by at least two different scanning procedures: (1) varying Ω at a fixed F (frequency scanning) and (2) varying F at a fixed Ω (amplitude scanning) with μ and g as fixed parameters. The thresholds in terms of controlled parameters F vs Ω are shown in Fig. 2. This figure is referred to as a state diagram. The diagram covers the transition thresholds in the fundamental ($\lambda=1$) and subharmonic locking ($\lambda=1/2$). The curves denoted as $L(\lambda)$ are the boundaries from the quasiperiodic to the locked state and $QP(\lambda)$ are from locked to the quasiperiodic state, respectively, with the winding number λ. The wide variety of features in the state diagram are summarized in Sec. III A and the dynamical transitions of the attractors are elucidated in Sec. III B. The distinctions of the state diagram among Eq. (3), Duffing, and VDP are provided in Sec. III C for the sake of exploiting the influences of the nonlinear restoring force on the bifurcation structure.

A. Phenomena of steady states

1. Arnold tongues and Farey tree

The free-running frequency of the circuit is at $\Omega_s=0.8355$ (135.525 Hz) without an external force and is pulled toward the external one as the external strength is increased. More power is required to lock the frequency as the driving frequency is farther away from the Ω_{s0}. The locked threshold appears as a tongue with the tip at Ω_s, denoted as the Arnold tongue. As the force F is above curve $L(1)$, the dynamical behaviors are found to

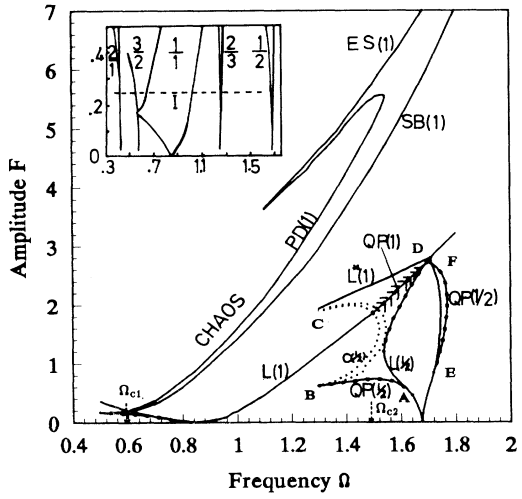

FIG. 2. The state diagram with parameters $\mu=0.1$, $g=-1$, $\alpha=1$, $\gamma=0.1$, and $0.4<\Omega<1.8$. Curves $L(\lambda)$, QP(λ), SB(λ), and $C(\lambda)$ are the thresholds of injection locking, quasiperiodic, symmetry breaking, and crisis, respectively, with winding number λ. Curve PD(λ) is the threshold of the first period doubling. Curve ES(λ) is the threshold for solutions escaping from the potential well.

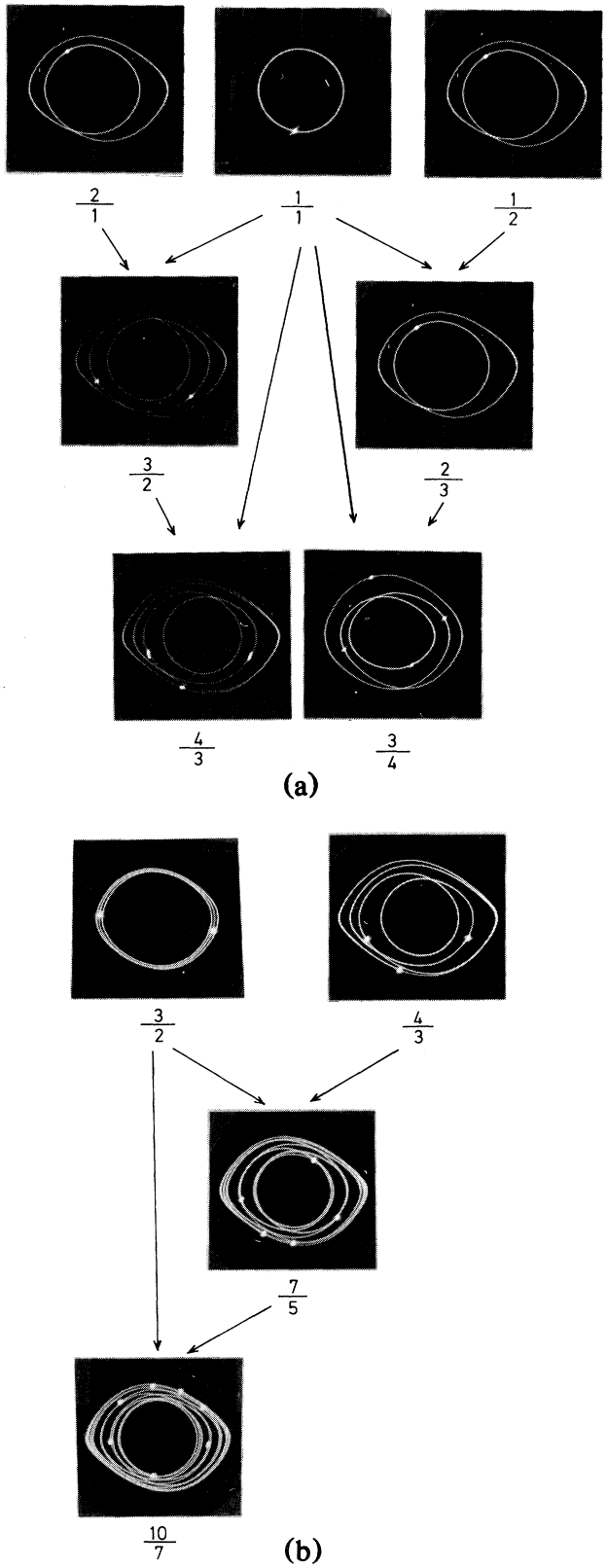

FIG. 3. Farey sequence for (a) $\lambda=1/2$, 2/3, 3/4, 1/1, 4/3, 3/2, and 2/1 with $F=0.25$ and (b) $\lambda=3/2$, 10/7, 7/5, and 4/3 with $\Omega=0.554$. The number of dot points accounts for the driving periods.

be similar to those in Duffing equation. This is verified by the swallow-tailed shape of the boundaries, which are already known in the Duffing oscillator [4]. The generic properties, such as hysteresis and boundary crisis, occurring in the swallow-tailed transitions are also observed in this case.

Except for the major tongues with $\lambda=1$ or $1/2$, several small locking islands with ultrasubharmonic resonance are located within the quasiperiodic sea. Some of them are presented in the inset of Fig. 2. Their presence leads to the universal feature of the Farey tree in winding numbers. Figures 3(a) and 3(b) illustrate a sequence of the phase portraits with winding numbers which satisfy the rule of the Farey trees in frequency scanning with $F=0.25$ and in amplitude scanning with $\Omega=0.554$, respectively.

2. *Symmetry breaking and period-doubling route*

The route to chaos follows the scenario of period doubling (or flip bifurcation) once the state becomes locked. The winding number remains constant during the cascade of period doubling. In the fundamental tongue, two attractors with the phase portraits asymmetrical with respect to the origin are first observed as the driving force reaches above the threshold of SB(λ). This is true despite the fact that Eq. (3) is symmetrical under the transformation with $x\rightarrow -x$ as $t\rightarrow t+\pi$. The route is preceded by the bifurcation of symmetry breaking (SB). This is an important precursor for the period-doubling route and belongs to the pitchfork bifurcation. Whereas no SB threshold is observed in the subharmonic tongue because the attractor is inherently asymmetrical with approximately 180 ° phase difference in their solutions. The final attractor depends on the choice of the initial condition and has its own period-doubling (PD) route to chaos. The respective thresholds of the subsequent bifurcations are observed to be slightly different and are folded back at high excitation, such as PD(1) in Fig. 2. The deviation in the thresholds gives rise to varieties of chaotic transitions, which are detailed in Sec. III B.

3. *Multistability and swallow-tailed bifurcation structure of subharmonic locking*

The thresholds in the subharmonic region are quite-complicated, despite the small damping coefficient μ in Eq. (3). A part of curve $L(1)$ is next replaced by QP(1) (dotted line) and is observed by the downward scanning with initial state above the $L^*(1)$ as the driving frequency reaches above the critical frequency Ω_{c2}, determined from the intersection of curve $L(1)$ and crisis threshold $C(1/2)$. Six tails denoted as A, B, C, D, E, and F can be observed from the different dynamical features. The tails A, D, E, F are related to hysteresis, and the tails B and C are related to crisis. Double hysteresis loops by amplitude scanning are detailed in Fig. 4 with $\Omega=1.57$ on the left-hand side of the tip. Tails E and F appear as an almost vertical zone on the right-hand side of the tip. Here, the behavior of bistability is thus much easier to be found by frequency scanning than by amplitude scanning.

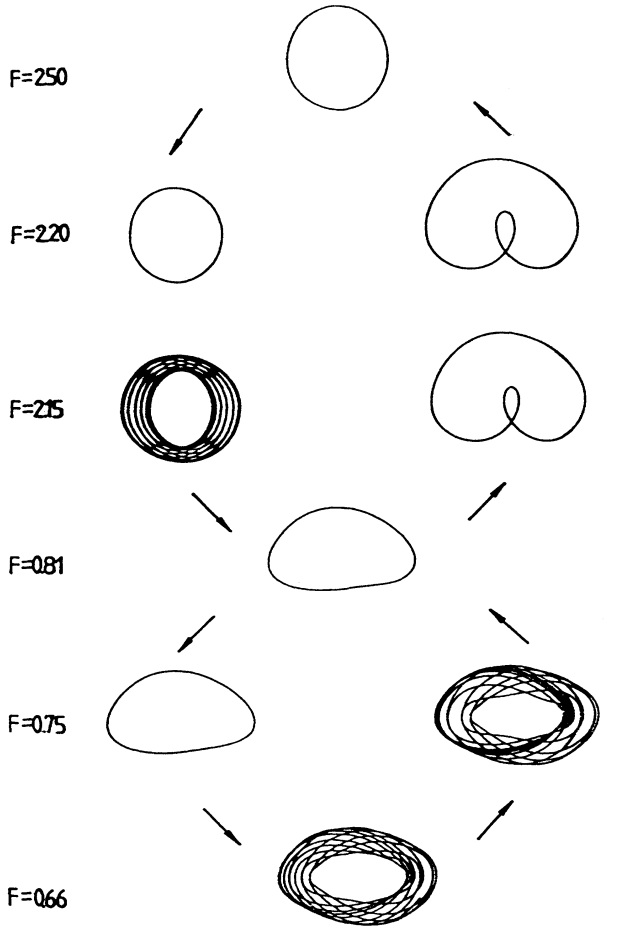

FIG. 4. The phase portraits of double hysteresis loop with $\Omega=1.57$ in the subharmonic region. The arrows stands for the direction of amplitude scanning.

B. Bifurcations with intermittent and blue-sky catastrophes

The complicated behaviors due to the presence of the cubic term in the nonlinear force are confirmed from the state diagram. From the bifurcation viewpoint, there are six common types of bifurcations—saddle node (hysteresis), pitchfork (symmetry breaking), flip (period doubling), intermittent catastrophe (injection locking type I), blue-sky catastrophe (injection locking type II), and inverse Hopf (injection locking type III) in the observed case. This complexity originates from the existence of the saddle point, which divides the whole basin into two smaller ones. The transient processes of the quasiperiodic attractors, which have something to do with the saddle point, are examined in the following. The catastrophic transitions of chaotic attractors are also presented.

1. *Injection locking*

First, the transient process near the tip of the fundamental tonque is examined. Figures 5(a) and 5(b) show the typical return maps with driving frequencies on both sides of Ω_{s0} at $\Omega=0.75$ and $F=0.065$ or $\Omega=0.9$ and

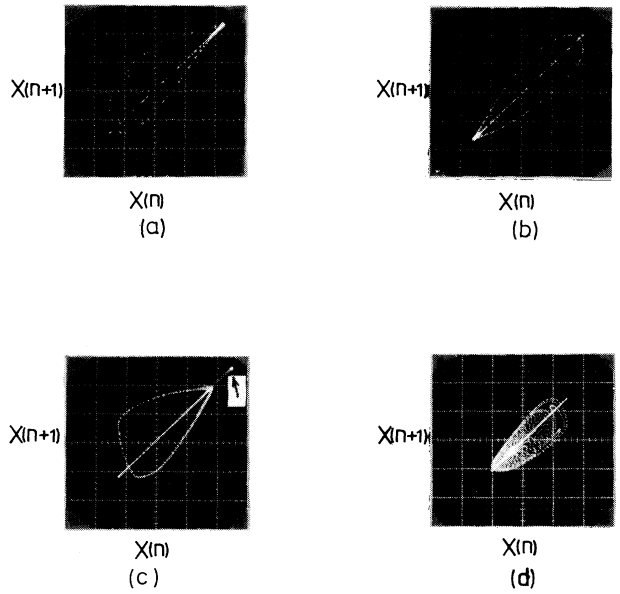

FIG. 5. The return map with driving frequency at (a) $\Omega=0.75$ and $F=0.065$, (b) $\Omega=0.9$ and $F=0.0495$, (c) $\Omega=0.7$ and $F=0.104$, and (d) $\Omega=0.99$ and $F=0.171$.

$F=0.0495$, respectively. Before locking in the quasiperiodic state, the maps form closed loops with the mapping points progressing intermittently, and reveal the dense sets near the diagonal. These dense sets form a concave curve and is tangential to the diagonal. As the external force becomes strong enough, a pair of saddle and node develops such that the quasiperiodic attractor rapidly shrinks to the node, which is near the original attractor. This process is an intermittent catastrophe and is referred to as type-I injection locking.

As the frequency is tuned to within the region of hysteresis loop, a different capture process is observed. The typical feature of return map is shown in the Fig. 5(c) with $F=0.104$ and $\Omega=0.7$ near curve $L(1)$. The existence of hysteresis implies that the saddle point is initially away from the quasiperiodic attractor. According to our observation, the attractor is enlarged and then touches topologically the inset of the saddle as the force is on curve $L(1)$. The transient almost along the diagonal implies that the attractor, once touching the inset, is absorbed immediately toward the saddle point and is then repelled along the outset to a new attractor (arrow), which is far away from the old one. This phenomenon is referred to as a blue-sky catastrophe (type-II injection locking) since the quasiperiodic attractor escapes into the blue sky [2]. In the reverse scanning, the locked state becomes quasiperiodic via saddle-node bifurcation as F is below curve QP(1). The cusp frequency of hysteresis loop acts as the border of type-I and -II injection locking along the frequency axis. The transient process becomes very slow as the injection frequency is farther away from the tip in the intermediate region. The bifurcation is confirmed to be a inverse Hopf bifurcation (type III) with a pair of complex multipliers crossing the unit circle. A typical return map is shown in Fig. 5(d) with $F=0.171$ and $\Omega=0.99$. The calculated multipliers are equal to $0.698\pm0.716j$. The return map is folded and complicated during the transient. No hysteresis loop is observed during the amplitude scanning.

These processes can also be observed in the subharmonic resonant region. For example, the blue-sky catastrophe is found as F is backward scanned from QP(1) down to $L(1/2)$ (dotted section). The return map and Poincaré section are shown in Figs. 6(a) and 6(b) with $\Omega=1.668$. The digit-8 attractor settles down rapidly to a different attractor with two points distributed on the opposite side of the diagonal. Topologically, the old attractor touches the inset of the saddle-point manifold and follow the outset to the new stable nodes. Owing to the subharmonic, the escaping comes from the direction which is normal to the diagonal in the return map $x(n+1)$ vs $x(n)$.

2. *Transitions of chaotic attractors*

The transitions for the chaotic attractors are next examined. The shape of the chaotic attractor developed via the period-doubling route looks similar to the logistic map. The boundary crises of the chaotic attractor happen as the parameters reach curve $C(\lambda)$, where the boundary of the chaotic attractor touches the unstable

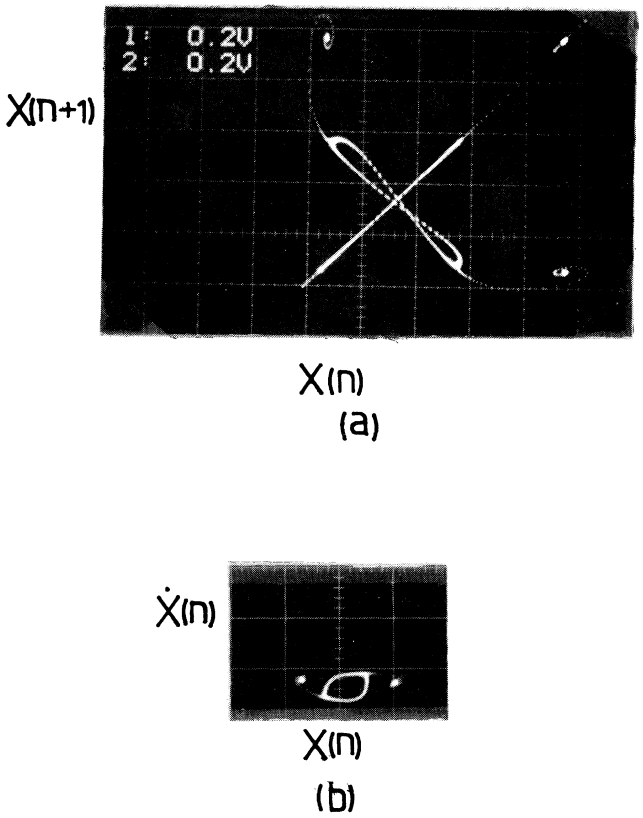

FIG. 6. (a) The return map and (b) Poincaré section of the blue-sky catastrophe for the quasiperiodic state at $F=2.59$ and $\Omega=1.668$ in the subharmonic region.

fixed point [23]. The instability is confirmed from the slope of the interception point of the map with the diagonal. Three kinds of transition outcomes are observed, depending on the frequency. As $\Omega < \Omega_{c1}$ in the fundamental tonque, the chaotic attractor is indicated from Fig. 7(a) to suddenly disappear and a new QP attractor appears with $F=0.170$ and $\Omega=0.5$. For $\Omega > \Omega_{c1}$, the chaotic attractor hops to the other chaotic attractor rather than a quasiperiodic attractor. The Pomean and Manneville (PM) intermittency is observed to occur from Fig. 7(b) as the parameters are increased deep into the chaotic region with $\Omega=1.141$ and $F=2.47$ [24]. The dense set (arrow) is inversely tangential to the diagonal just as the prediction of PM intermittency. The last transitional outcome switches to the attractor with period one as in Fig. 7(c). This situation arises at high excitations, where the chaotic state and locked state coexist at the same parameters.

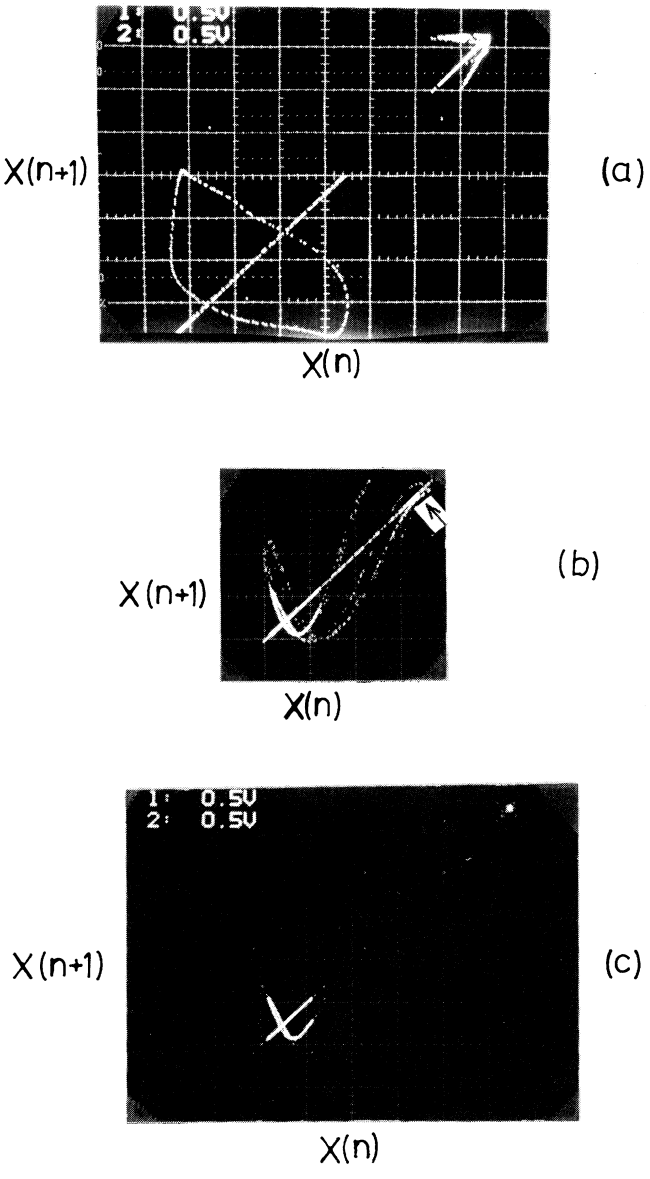

FIG. 7. The return maps for the different kinds of crisis events with (a) $F=0.170$ and $\Omega=0.5$, (b) $F=2.47$ and $\Omega=1.141$, and (c) $F=4.91$ and $\Omega=1.48$.

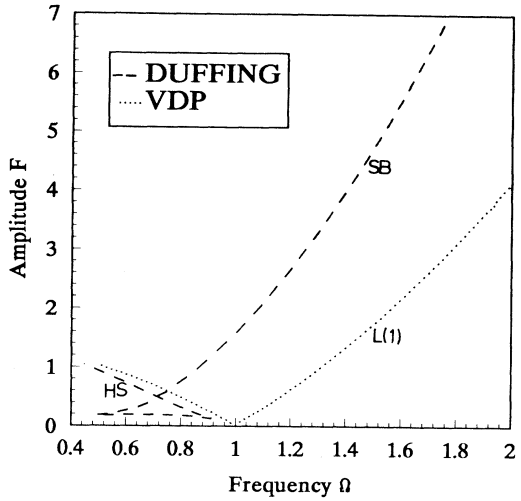

FIG. 8. The state diagrams of Van der Pol ($\mu=0.1$, $g=-1$, and $\alpha=1$) and Duffing ($\mu=0.1$, $\alpha=1$, and $\gamma=0.1$) oscillators. SB is the threshold of symmetry breaking and HS is the threshold of hysteresis in Duffing oscillator.

C. Comparisons in the bifurcation structure with Duffing and VDP oscillators

The bifurcation structures for the Duffing oscillator [Eq. (1)] and VDP [Eq. (2)] are illustrated in Fig. 8 for the sake of comparison. Compared to VDP, the tonque in Eq. (3) is more asymmetrical with curve $L(1)$ considerably reduced in the left-hand side of the tip. The frequency acquisition occurs more easily in the lower-frequency side than in the high one. This is due to the negative sign in the cubic term of the nonlinear restoring force so that the natural frequency always shifts downward as the excitation is increased. The thresholds for the lock and out of lock are different in Eq. (3) and form a hysteresis loop. The locking threshold $L(\lambda)$, from a comparison with the Duffing oscillator, belong to the global blue-sky catastrophe rather than the local saddle-node bifurcation. This phenomenon is commonly observed in a radio receiver with a phase-locked-loop circuit. The transitions in the subharmonic region are much more complicated than those of Eqs. (1) and (2), where no subharmonic transitions are present. It can be ascribed to the strong interactions between the nonlinear restoring and damping terms.

IV. CONCLUSIONS

The bifurcations in self-oscillation systems were extensively investigated in this paper with their potential application for the Van der Pol oscillator containing a nonlinear restoring force. The dynamical behaviors of the Farey tree, locking transients, and chaotic transitions were especially focused upon. With the presence of a

nonlinear force term, the exotic saddle point was created and, consequently, sped up the capture process during frequency acquisition. Three varieties of the capture process from quasiperiodic to locked state could be clarified as intermittency catastrophe, blue-sky catastrophe, and inverse Hopf bifurcation. It was concluded that, with the coexistence of nonlinear restoring and damping terms, the most eminent behaviors not observed in VDP and Duffing oscillators were the intermittency catastrophe, the blue-sky catastrophe, and complicated bifurcations of subharmonic regions.

ACKNOWLEDGMENTS

The study was supported by the National Science Council, Republic of China under Contract No. NSC 81-0208-M-009-19. The authors would like to thank Mr. T. Knoy for his comments on the manuscript. C.S.W. also thanks Telecommunication Laboratory, Ministry of Transportation and Communication, for their support in the continuation of this work.

---

*FAX: 886-35-710116.

[1] C. Hayashi, *Nonlinear Oscillations in Physical Systems* (McGraw-Hill, New York, 1964), Chaps. 12 and 13.

[2] J. M. Thompson and H. B. Stewart, *Nonlinear Dynamics and Chaos: Geometrical Methods for Engineers and Scientists* (Wiley, New York 1987), Chap. 13.

[3] B. A. Huberman, Phys. Rev. Lett. **43**, 1743 (1979).

[4] C. S. Wang, Y. H. Kao, J. C. Huang, and Y. S. Gou, Phys. Rev. A **45**, 3471 (1992).

[5] J. M. T. Thompson, Proc. R. Soc. London Ser. A **421**, 195 (1989).

[6] N. Krylov and N. Bogoliuboff, *International Nonlinear Mechanics,* Annals of Mathematics Ser. No. 11 (Princeton Univ. Press, Princeton, 1947).

[7] J. E. Flaherty and F. C. Hoppensteadt, Stud. Appl. Math. **58**, 5 (1978).

[8] J. Gugenheimer, Physica D **1**, 227 (1980).

[9] J. Grasman, Q. Appl. Math. **38**, 9 (1980).

[10] Y. Ueda and N. Akamatsu, IEEE Trans. Circuit Syst. **28**, 217 (1981).

[11] W. H. Steeb and A. Kunick, Int. J. Non-Linear Mech. **22**, 349 (1987).

[12] U. Parlitz and W. Lauterborn, Phys. Rev. A **36**, 1428 (1987).

[13] G. R. Qin, D. C. Gong, R. Li, and X. D. Wen, Phys. Lett. A **141**, 412 (1989).

[14] H. A. Haus, *Waves and Fields in Optoelectronics* (Prentice-Hall, Englewood Cliffs, NJ, 1984), Chap. 10.

[15] P. J. Probert and J. E. Carroll, IEEE Proc. **134**, 295 (1987); **136**, 22 (1989).

[16] M. Okuda, Prog. Theor. Phys. **66**, 90 (1981).

[17] D. L. Gonzalez and O. Piro, Phys. Rev. Lett. **50**, 870 (1983).

[18] S. Rajasekar and M. Lakshmanan, Physica D **32**, 146 (1988).

[19] M. Feingold, D. L. Gonzalez, O. Piro, and H. Viyurro, Phys. Rev. A **37**, 4060 (1988).

[20] D. Armbruster and G. Dangelmayr, Phys. Lett. A **138**, 46 (1989).

[21] J. Maelko and H. L. Swinney, Phys. Lett. A **119**, 403 (1987).

[22] M. H. Jensen, P. Bak, and T. Bohr, Phys. Rev. Lett. **50**, 1637 (1983).

[23] G. Grebogi, E. Ott, and J. A. Yorke, Phys. Rev. Lett. **48**, 1507 (1982).

[24] P. Manneville and Y. Pomean, Phys. Lett. **75A**, 1 (1979).

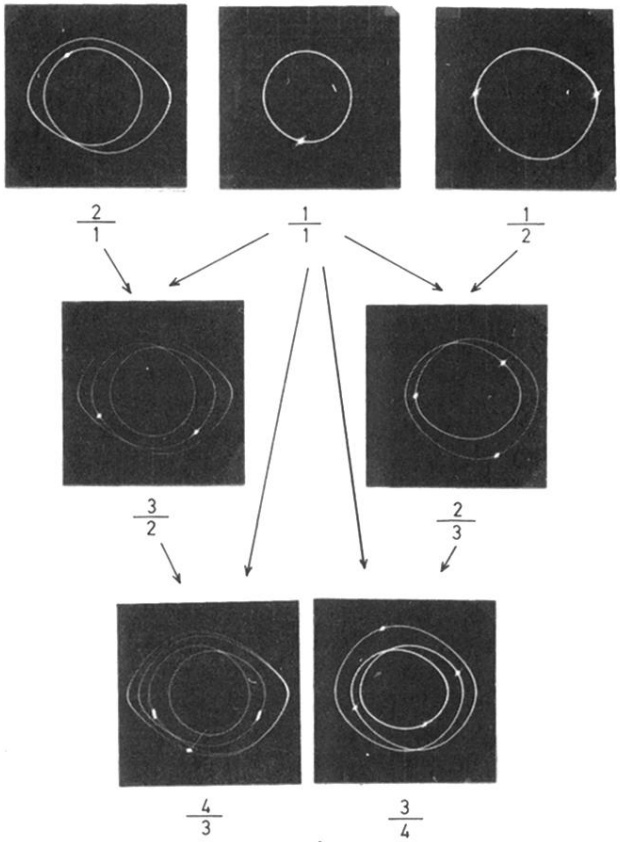

FIG. 3. Farey sequence for (a) $\lambda=1/2$, 2/3, 3/4, 1/1, 4/3, 3/2, and 2/1 with $F=0.25$ and (b) $\lambda=3/2$, 10/7, 7/5, and 4/3 with $\Omega=0.554$. The number of dot points accounts for the driving periods.

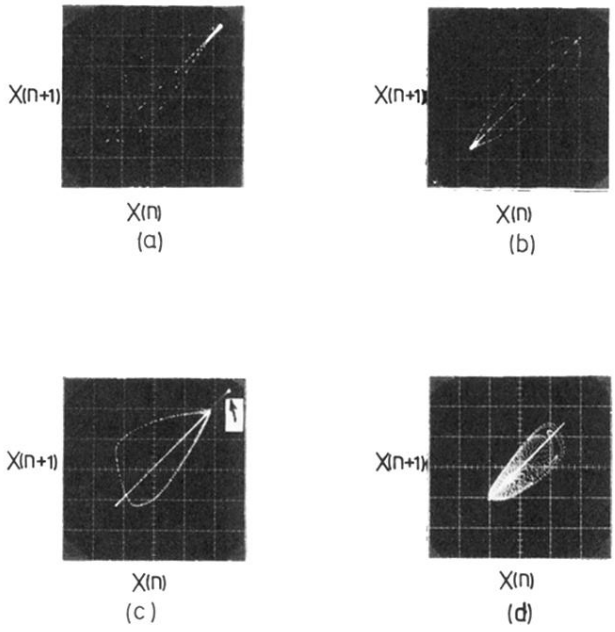

FIG. 5. The return map with driving frequency at (a) $\Omega=0.75$ and $F=0.065$, (b) $\Omega=0.9$ and $F=0.0495$, (c) $\Omega=0.7$ and $F=0.104$, and (d) $\Omega=0.99$ and $F=0.171$.

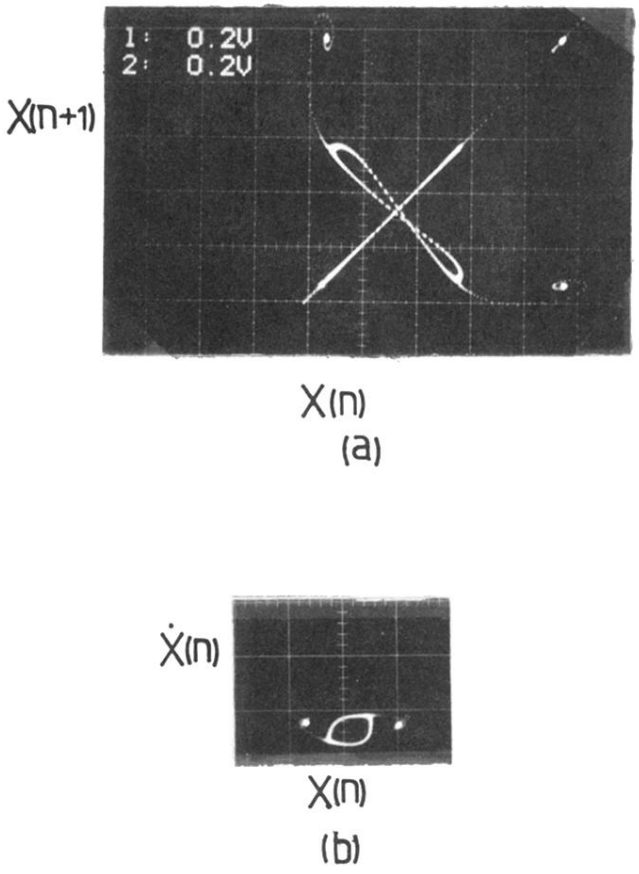

FIG. 6. (a) The return map and (b) Poincaré section of the blue-sky catastrophe for the quasiperiodic state at $F=2.59$ and $\Omega=1.668$ in the subharmonic region.

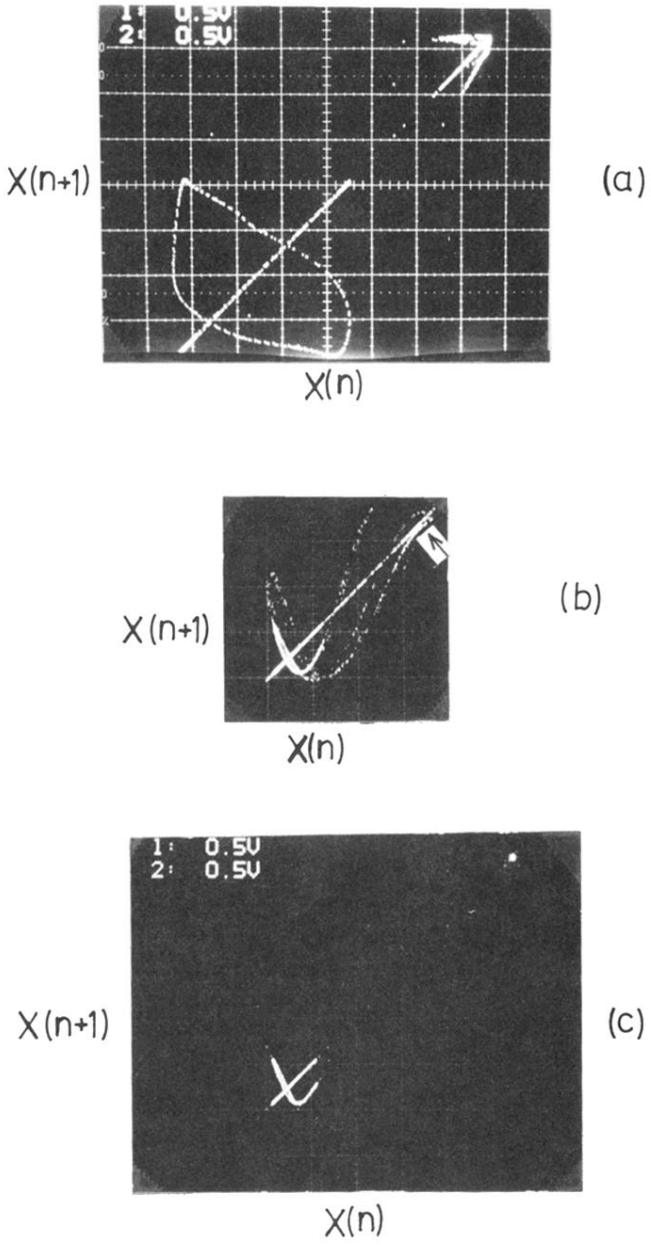

FIG. 7. The return maps for the different kinds of crisis events with (a) $F=0.170$ and $\Omega=0.5$, (b) $F=2.47$ and $\Omega=1.141$, and (c) $F=4.91$ and $\Omega=1.48$.